COMMUNICATION

Hybrid Benzidinium Lead Iodide Perovskite with 1D structure as Photoinduced Electron Transfer Photocatalyst

Received 00th January 20xx,
Accepted 00th January 20xx

DOI: 10.1039/x0xx00000x

Yong Peng,[a] Josep Albero,[a]* Eleuterio Álvarez[b] and Hermenegildo García[a]*

A hybrid benzidinium lead iodide perovskite (formula PbI_3benzidinium$_{0.5}$) (3) with 1D structure has been synthesized and characterized. The hybrid perovskite exhibits visible light (λ >450 nm) photocatalytic activity to promote the photoinduced electron transfer cis-to-trans isomerization of stilbene. The solid photocatalyst undergoes change in the particle morphology, but maintains the crystallinity.

Introduction

The excellent charge separation efficiency and charge mobility in hybrid methylammonium lead iodide perovskite is responsible for the high efficiency of solar cells using this type of perovskite as photoactive material.[1, 2] Solar to current efficiencies over 20 % have been certified for some of these photovoltaic devices based on methylammonium lead iodide perovskite.[3, 4] Besides light absorption in the whole UV-vis spectral range, one of the key features for the excellent photo response is the low exciton binding energy, that is responsible for a very efficient charge separation.[5]

The optoelectronic properties of hybrid lead iodide perovskites that have been determined as highly relevant in photovoltaic devices are also wanted for other possible applications of these materials and, particularly, in photocatalysis. However, up to now, reports on the use of hybrid perovskites in photocatalysis are very limited,[6, 7] probably due to the lack of stability of hybrid perovskites in most of the media typically used in photocatalysis, particularly in water and polar solutions.

Another aspect to be considered for the potential application of hybrid perovskites beyond photovoltaics is the possibility to modify their chemical composition, introducing other organic ammonium cations that could play a specific role promoting charge separation.[8, 9]

Aimed at exploiting the possibilities that hybrid organic lead iodides offer in the field of photocatalysis, the present study reports the preparation of the hybrid lead iodide perovskite of the benzidine di-protonated salt, finding that the resulting hybrid perovskite exhibits photocatalytic activity for the photoinduced electron transfer cis-to-trans isomerization of stilbene. Benzidine diammonium was selected as organic cation due to the known ability of biphenyl in molecular organic photochemistry to increase the efficiency of photoinduced electron transfer processes by favouring charge separation.[10, 11] The long lifetime of biphenyl radical ions in the microsecond time scale allows their reaction with substrates promoting electron transfer processes.

Results and Discussion

Material preparation and characterization

The diammonium salt of benzidine was prepared in two steps: starting from commercial hydrazobenzene by acid-catalyzed rearrangement to benzidine **(1)**, then, by careful protonation of **1** with an excess of concentrated aqueous HI acid. The structure of product **1** was confirmed by ^{1}H NMR and IR spectroscopy (see Fig. S1 and S2 in supplementary information). Particularly, remarkable changes in the symmetry and chemical shifts of the aromatic protons respect to parent hydrazobenzene were recorded in ^{1}H NMR spectroscopy of compound **1**. Specifically, benzidine 1 exhibits two doublets corresponding to a A_2M_2 system appearing at 6.77 and 7.27 ppm corresponding to the aromatic protons at *ortho* and *meta* position of the amino groups. In IR spectroscopy benzidine **1** exhibits two vibration peaks at 3400 and 3250 cm^{-1} attributed to a primary amine.[12] The resulting salt **2** was characterized by combustion elemental analysis (Table S1 in supplementary information) and by IR spectroscopy. A good match between elemental composition determined by combustion analysis and the theoretical value based on the molecular formula corresponding to the disalt **2**,

[a] *Instituto Universitario de Tecnología Química CSIC-UPV, Universitat Politècnica de València, Avda. De los Narajos s/n 46022, Valencia (Spain). E-mails: joalsan6@itg.upv.es and hgarcia@qim.upv.es; Tel: +34 963877807.*
[b] *Departamento de Química Inorgánica, Instituto de Investigaciones Químicas CSIC-US. Av. Américo Vespucio 49, 41092, Sevilla (Spain).*
Electronic Supplementary Information (ESI) available: [details of any supplementary information available should be included here]. See DOI: 10.1039/x0xx00000x

combined with the broad peak near 3000 cm^{-1} and the disappearance of the double peak around 3500 ~ 3200 cm^{-1} in IR spectrum of salt **2** indicate the formation of benzidinium diiodide. The aforementioned benzidinium lead iodide perovskite (**3**) was, then, obtained by mixing in DMF, the corresponding amount of lead iodide (PbI_2) and benzidinium cation **2**. Precipitation of the solid perovskite **3** as a fine powder can be achieved by addition of toluene. Single crystals of the same hybrid perovskite **3** suitable for XRD structural characterization could be

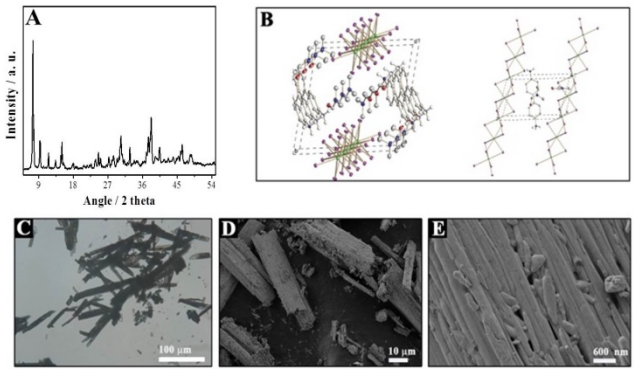

Fig. 1. (A) XRD patterns of **3** fine powder. (B) Two views (ORTEP representation) of crystal structure of PbI_3bezidinium$_{0.5}$ determined by single crystal-XRD with thermal ellipsoids set at a 30 % probability level. The hydrogen atoms and one part of modelling of a disordered DMF solvent molecule are omitted for clarity (CCDC 1902819). (c) Optical microscopy image of perovskite **3** crystals. and (D)-(E) SEM image of material **3** as fine powder.

obtained by slow diffusion of toluene vapors into the DMF solution of PbI_2 and **2**, allowing the slow precipitation of fine yellow needle-like crystals to occur during one day.

Chemical analysis of the hybrid PbI_3(**2**)$_{0.5}$ (material **3)** was carried out combining combustion elemental analysis for C, H and N elements with ICP-OES analysis of Pb (Table S2 in supplementary information) and assuming that the residual percentage is due to the sum of I and O. It was also considered that a perovskite **3** unit formula contains 0.5 molecules of **2** to maintain neutrality. Then, the analytical data lead to the experimental formula PbI_3(**2**)$_{0.5}$(DMF)$_{0.3}$ (See supporting information for a detailed calculation), indicating that the present material can be reasonably considered as a defectless hybrid perovskite. The proposed PbI_3(**2**)$_{0.5}$(DMF)$_{0.3}$ formula for perovskite **3** is within the accepted error for experimental analytical data of ± 0.4 %.

Single crystal XRD indicates that the structure of benzidinium lead perovskite **3** is constituted by parallel chains of PbI_6 octahedra sharing the faces aligned along the long axis of the crystal that are coordinated to dications **2** that interact by Coulombic forces and hydrogen bonding with the PbI_6 octahedra. Benzidine diammonium ions establish among them van der Waals forces due to π - π stacking of the aromatic rings. The PbI_6 and dication **2** chains define channels that are occupied by DMF molecules that interact through hydrogen bonds with PbI_6 and dications **2**. Fig. 1 presents two views of the structure corresponding to material **3** prepared in this study. The crystal data, structure refining, crystal drawing of different views and partial packing diagram can be found in Table S3, Fig. S3 and Fig. S4, respectively, in supplementary information. Overall, the structure for PbI_3(**2**)$_{0.5}$ corresponds to a 1D hybrid perovskite. It is well established in the field of hybrid perovskites that the size of the organic cation determines the structure of the perovskite.[13] Only methylammonium and formamidinium, the smallest organic ammonium ions, are able to form hybrid perovskites with 3D structure. These structures are transformed into 2D or 1D when the size of the organic cation becomes larger. In particular, it has been reported that phenylammonium lead iodide is a 2D perovskite,[14] while in the present case the structure of solid **3** corresponds to a 1D material.

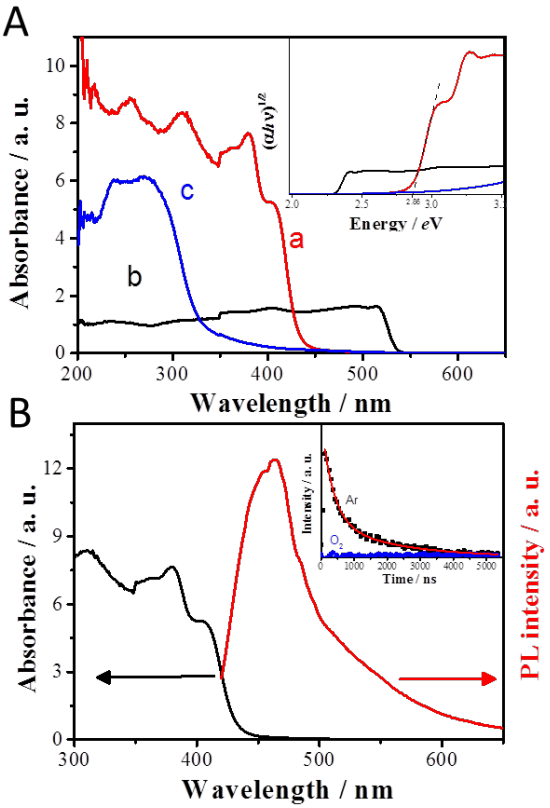

Fig. 2. (A) Diffuse reflectance UV-Vis spectra of hybrid perovskite **3** (a), PbI_2 (b), and Benzidinium diiodide **2** (c). Inset: Tauc plot corresponding to the absorption spectrum. (B) Diffuse reflectance absorption(black) and emission (red) spectra of hybrid perovskite **3** upon excitation at 390 nm. Inset: temporal emission profile of hybrid perovskite **3** monitored at 465 nm under Ar atmosphere (black dots) and in the presence of O_2 (blue dots). The red line corresponds to bi-exponential fitting.

The benzidinium perovskite **3** was sensitive to the temperature above 70 °C (Fig. S5 in supplementary information) and also depending on the nature of the solvent it shows a limited stability in solution (Fig. S6 in supplementary information). However, it was found that the benzidinium perovskite **3** is indefinitely stable in hexane and also can stand toluene for a few hours, in contrast, material **3** dissolves partially in H_2O and acetonitrile. Therefore, although limited, there is a range of conditions and solvents in which perovskite **3** can be employed.

The 1D structure of perovskite **3** is reflected in the morphology of the crystals. According to optical microscopy, the solid **3** is constituted by needles and rods of millimetric dimensions and high aspect ratio. SEM images show that the rods are

constituted by the agglomeration of thin needles of about 200 nm width and very long length about 50 µm. Much smaller debris due to the breaking of the needles can also be observed in the images. Besides optical microscopy, Fig. 1 also shows some representative SEM images of material **3**.

The 1D structure of the benzidinium hybrid perovskite **3** is also reflected in the optical absorption spectrum of the material. 3D perovskites exhibit a continuous absorption band in most of the visible range. In contrast, the onset of the 1D and 2D hybrid perovskite occurs in the visible region. The diffuse reflectance UV-Vis spectrum of the benzidine perovskite **3** is presented in Fig. 2. As can be seen there, the onset of the absorption spectrum of the hybrid perovskite is about 450 nm, the corresponding Tauc plot indicates that the bandgap of the benzidinum lead perovskite **3** is 2.86 eV.

It is well-known in the state of the art that a change in the structure of the hybrid perovskite from 3D to lower dimensionality originates an increase in the bandgap.[15] Thus, typical 3D $MAPbI_3$ (MA: methylammonium) perovskite reports a 1.51 eV band gap, while 2D $BDAPbI_3$ (BDA: di-cation of 1,4-diaminobutane) perovskite has reported 2.37 eV.[16, 17] The hybrid perovskite **3** exhibits a strong photoluminescence with partially resolved fine structure with an emission maximum at 463 nm, when the material is excited at 390 nm (Fig. 2). The temporal profile of the emission under argon can be fitted to a biexponential decay with a short-lived component with τ_1 = 344 ns, contributing about 15 % to the total emission intensity and a much longer-lived component with τ_2 = 1974 ns and a contribution of 85 %. This emission is totally quenched in the presence of O_2, and accordingly it can be assumed that it derives from electron-hole recombination.[18] In this regard, the biexponential kinetics can be rationalized considering that charge carriers responsible for the long-lived emission are those located in trap sites, thus prolonging their life.

Photocatalytic activity

As indicated in the introduction, the purpose of the study was to explore the possible application of the optoelectronic properties of hybrid perovskites in photocatalysis. Since material **3** should exhibit photoinduced charge separation through photoexcitation, it was selected as photocatalyst for a process that can be considered as a model reaction for photoinduced electron transfer, namely, cis-to-trans stilbene photoisomerization.[19] This geometrical isomerization of stilbene was extensively studied in the context of photoinduced electron transfer processes promoted by organic photosensitizers, there being extensive literature proving the reaction mechanism.[20-22]

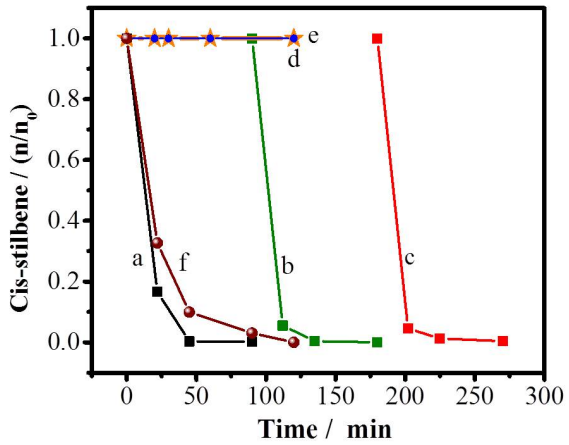

Fig. 3.Cis-to-trans stilbene isomerization promoted by visible light (λ > 450 nm) in the presence of perovskite **3** acting as photocatalyst (a). Plots b and c correspond to consecutive reuses of the photocatalysts. Control experiments carried out under the same conditions but in the absence of **3** (d), in the dark in the presence of **3** (e) or in the presence of MAPbI perovskite instead of **3** (f).

Preliminary blank controls by long-wavelength irradiation of cis-stilbene with visible light (λ > 450 nm) show that no cis-to-trans isomerization occurs in the absence of perovskite **3** under the irradiation conditions. Also, control experiments in the dark, but in the presence of hybrid perovskite **3** show no cis-to-trans isomerization (Fig. 3 (d) and (e)).

In contrast, upon visible light irradiation of a solution of cis-stilbene in hexane in the presence of hybrid perovskite **3** (0.25 mmol/mL) a complete cis-to-trans isomerization was observed after 1 h irradiation. To put the photocatalytic activity of perovskite **3** into context, the well-known methyl ammonium lead iodide perovskite ($MAPbI_3$) was also evaluated as photocatalyst to promote the cis-to-trans stilbene isomerization under identical conditions as those employed in the case of perovskite **3**. As can be seen in Fig. 3 (f), although complete cis-to-trans isomerization was also achieved using $MAPbI_3$ as photocatalyst, the reaction kinetics was slower in this case as compared to perovskite **3**. This shows the benefits of the benzidine diammonium unit in the photocatalytic activity of the resulting hybroid perovskite. Fig. 3 shows the temporal profile of the photoinduced cis-to-trans isomerization. As can be seen there, upon selective irradiation of perovskite **3**, photoinduced electron-hole separation should occur. Holes on the perovskite would abstract one electron from cis-stilbene, leading to the generation of the corresponding stilbene radical cation that would undergo isomerization to the trans-stilbene radical cation. Back electron transfer from hybrid perovskite to the photocatalyst would complete the mechanism. The key mechanistic step is the cis-trans equilibrium of stilbene radial cation as a consequence of the lower bond order. The process is illustrated in the Scheme 1.

After the reaction, the sample of perovskite **3** used as photocatalyst was characterized by XRD and SEM (Fig. 4). XRD reveals changes in the diffraction pattern, although crystallinity was maintained. Unfortunately, the used sample **3** was not suitable for single-crystal diffraction. SEM images show that during the reaction a remarkable change in the morphology of the particles occur. It seems that the rods constituted by agglomeration of thin needles initially present in the fresh

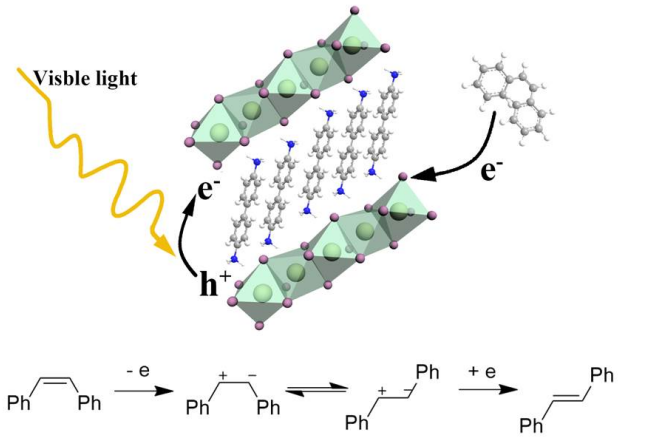

Scheme 1 Schematic diagram for photoinduced cis-to-trans stilbene isomerization process and the proposed mechanism.

sample have undergone extensive deaggregation during photochemical reaction. It is worth commenting that analogous deaggragation under irradiation has also been observed in carbon nanotube and attributed to the Coulumbic repulsion between photoexcited tube due to their charges.[23]

In spite of the morphological changes in the hybrid perovskite **3** during reaction, the photocatalytic activity of this photocatalyst remained unchanged, as consequence 3 consecutive resues of perovskite **3** were carried out without significant activity reduction as can be seen in Fig. 3 (b) and (c).

To further investigate the reason of the XRD pattern change, hybrid perovskite **3** was dispersed in hexane and then XRD patterns were recorded in the course of time (Fig. S8 in supplementary information). Surprisingly, the peaks at 2ϑ = 7.36º and 7.56º, which belongs to the (001) and (010) crystal plane of material **3** gradually disappeared, while the peak at 2ϑ = 7.75º became more intense, indicating that without stirring or light irradiation, the hybrid perovskite **3** suffered a structural change just when exposed in hexane. It should also be noted that the XRD patterns from material **3** after placed in hexane for 20 h are coincident with the patterns from material **3** after photoinduced isomerization reaction, which demonstrated that the structural change during the photoinduced isomerization is due to exposure to the solvent. The XRD patterns of photocatalyst **3** after each reuse are shown in Fig. S9 in supplementary information. As can be seen, no significant changes were found after the first use of the photocatalysts, thus, the XRD patterns after second and third use of **3** were very similar.

In order to gain some information about the reasons for the change in the XRD pattern and particularly if it is caused by the removal of DMF in the structure, perovskite **3** was submitted to vacuum at 50 ºC for 30 h, without observing noticeable changes in the XRD pattern as shown in Fig. S10 in Supplementary Information. It was expected that this treatment could remove DMF from the structure, but the lack of changes in the XRD pattern seems to rule out the wanted DMF removal. This is indicating that the most probable reason for structural change is due to the action of hexane or light or the combination of both.

In order to advance further in the understanding of the change of the XRD pattern, combustion and ICP analyses were carried out after stirring in the dark perovskite **3** in hexane for 7 h and submitting to reaction conditions (see Tables S4 and S5 in supplementary Information). The results show a decrease in the N-Pb ratio from 1.34 in the fresh sample to 1.17 after hexane stirring in the dark and to 0.92 after photocatalytic reaction. Considering that the theoretical N-Pb ratio of perovskite **3** in the absence of DMF should be 1, it can be concluded that perovskite **3** exposed to hexane suffers a partial loss of DMF molecules, while under reaction conditions the DMF molecules in the structure are completely removed.

Worth noticing is that, in addition, the diffuse reflectance UV-Vis spectrum of material **3** after dispersed in hexane also exhibited a typical perovskite absorption spectrum with a solvatochromic ~ 10 nm blue shift compared with the parent hybrid perovskite **3** as solid (Fig. S11 in supplementary information).

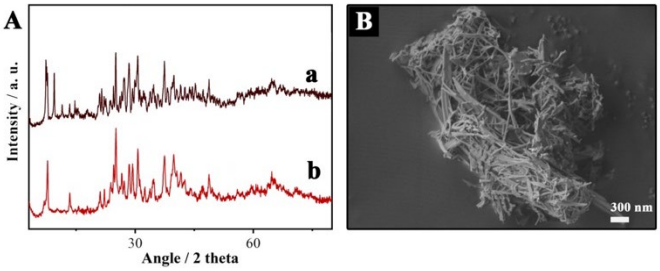

Figure 4. (a) XRD Patterns of Hybrid perovskite **3** before (a) and (b) after photoinduced isomerization reaction. (b) SEM image of the sample of hybrid perovskite **3** after photoinduced isomerization reaction.

Based on the small shift in the absorption spectrum and the structure of the single crystal of perovskite, it is reasonable to propose that the changes in the observed XRD pattern after dispersion in hexane are due to the removal of the DMF molecules from the void of hybrid perovskite **3** upon exposure to the hexane solvent. As a consequence, it is suggested that the XRD pattern changes after photoinduced isomerization reaction are the result of the loss of DMF molecules located in the void of hybrid perovskite **3** crystal.

Conclusions

The present study has shown the possibility to prepare hybrid lead iodide perovskite with benzidinium dication as organic moiety. The resulting perovskite has the specific formula $PbI_3(\mathbf{2})_{0.5}DMF_{0.3}$ including some DMF molecules from the synthesis in the structure. The hybrid material corresponds to 1D perovskite. This hybrid material **3** is stable in hexane and in this solvent, and can promote the photoinduced electron transfer cis-to-trans isomerization of stilbene. Although the material undergoes changes in the particle morphology and the XRD pattern during the photochemical reaction, it is proposed that these changes are the result of the loss of DMF

molecules. Moreover, these changes do not affect the photocatalytic activity of this photocatalyst. Overall, our study shows the potential of hybrid lead perovskites beyond the realm of solar cells and opens the way for an extensive application of this type of semiconducting materials as photocatalyst under conditions compatible with the structure.

Conflicts of interest

There are no conflicts to declare.

Acknowledgements

Financial support from the Spanish Ministry of Economy and Competitiveness (Severo Ochoa, and CTQ2015-69563-CO2-R1) and from the Generalitat Valenciana (Prometeo 2013-014) is gratefully acknowledged. Yong Peng also thanks the Universitat Politecnica de Valencia for a predoctoral scholarship.

Notes and references

1. A. Kojima, K. Teshima, Y. Shirai and T. Miyasaka, *J Am Chem Soc*, 2009, **131**, 6050-6051.
2. C. S. Ponseca, T. J. Savenije, M. Abdellah, K. Zheng, A. Yartsev, T. Pascher, T. Harlang, P. Chabera, T. Pullerits, A. Stepanov, J.-P. Wolf and V. Sundström, *Journal of the American Chemical Society*, 2014, **136**, 5189-5192.
3. M. Saliba, S. Orlandi, T. Matsui, S. Aghazada, M. Cavazzini, J.-P. Correa-Baena, P. Gao, R. Scopelliti, E. Mosconi, K.-H. Dahmen, F. De Angelis, A. Abate, A. Hagfeldt, G. Pozzi, M. Graetzel and M. K. Nazeeruddin, *Nature Energy*, 2016, **1**, 15017.
4. D. Zhao, C. Wang, Z. Song, Y. Yu, C. Chen, X. Zhao, K. Zhu and Y. Yan, *ACS Energy Letters*, 2018, **3**, 305-306.
5. T. M. Brenner, D. A. Egger, L. Kronik, G. Hodes and D. Cahen, *Nature Reviews Materials*, 2016, **1**, 15007.
6. S. Park, W. J. Chang, C. W. Lee, S. Park, H.-Y. Ahn and K. T. Nam, *Nature Energy*, 2016, **2**, 16185.
7. X. Zhu, Y. Lin, Y. Sun, M. C. Beard and Y. Yan, *J Am Chem Soc*, 2019, DOI: 10.1021/jacs.8b08720.
8. B. Febriansyah, T. M. Koh, R. A. John, R. Ganguly, Y. Li, A. Bruno, S. G. Mhaisalkar and J. England, *Chemistry of Materials*, 2018, **30**, 5827-5830.
9. H. Hu, F. Meier, D. Zhao, Y. Abe, Y. Gao, B. Chen, T. Salim, E. E. M. Chia, X. Qiao, C. Deibel and Y. M. Lam, *Advanced Materials*, 2018, **30**, 1707621.
10. P. B. Merkel, P. Luo, J. P. Dinnocenzo and S. Farid, *The Journal of organic chemistry*, 2009, **74**, 5163-5173.
11. E. Meggers, E. Steckhan and S. Blechert, *Angewandte Chemie International Edition in English*, 1995, **34**, 2137-2139.
12. R. A. Heacock and L. Marion, *Canadian Journal of Chemistry*, 1956, **32**, 1782-1795.
13. J. Albero, A. M. Asiri and H. García, *Journal of Materials Chemistry A*, 2016, **4**, 4353-4364.
14. P. Gao, A. R. Bin Mohd Yusoff and M. K. Nazeeruddin, *Nature Communications*, 2018, **9**, 5028.
15. D. H. Cao, C. C. Stoumpos, O. K. Farha, J. T. Hupp and M. G. Kanatzidis, *Journal of the American Chemical Society*, 2015, **137**, 7843-7850.
16. Y. Ogomi, A. Morita, S. Tsukamoto, T. Saitho, N. Fujikawa, Q. Shen, T. Toyoda, K. Yoshino, S. S. Pandey, T. Ma and S. Hayase, *The Journal of Physical Chemistry Letters*, 2014, **5**, 1004-1011.
17. M. Safdari, P. H. Svensson, M. T. Hoang, I. Oh, L. Kloo and J. M. Gardner, *Journal of Materials Chemistry A*, 2016, **4**, 15638-15646.
18. M. Lorenzon, L. Sortino, Q. Akkerman, S. Accornero, J. Pedrini, M. Prato, V. Pinchetti, F. Meinardi, L. Manna and S. Brovelli, *Nano Letters*, 2017, **17**, 3844-3853.
19. A. Corma, V. Fornés, H. García, M. A. Miranda, J. Primo and M.-J. Sabater, *J Am Chem Soc*, 1994, **116**, 2276-2280.
20. D. H. Waldeck, *Chem. Rev.*, 1991, **91**, 415-436.
21. S. G. Jack Saltiel, and Constance Werking, *The Journal of Physical Chemistry C*, 1986, **91**, 2755-2758.
22. M. de Wergifosse, A. L. Houk, A. I. Krylov and C. G. Elles, *J Chem Phys*, 2017, **146**, 144305.
23. M. Alvaro, C. Aprile, B. Ferrer and H. Garcia, *Journal of the American Chemical Society*, 2007, **129**, 5647-5655.